Solution pans and linear sand bedforms on the bare-rock limestone shelf of the Campeche Bank, Yucatán Peninsula, Mexico

John A. Goff[1*], Sean P.S. Gulick[1], Ligia Perez Cruz[2], Heather A. Stewart[3], Marcy Davis[1], Dan Duncan[1], Steffen Saustrup[1], Jason Sanford[1], and Jaime Urrutia Fucugauchi[2]

[1] Institute for Geophysics, Jackson School of Geosciences, University of Texas at Austin, USA

[2]Instituto de Geofísica, Universidad Nacional Autónoma de México, Ciudad Universitaria, Coyoacán, México

[3]British Geological Survey, Edinburgh, Scotland.

*Corresponding Author: University of Texas Institute for Geophysics, 10100 Burnet Rd Bldg 196-ROC, Austin, Texas USA 78758; email: goff@ig.utexas.edu; phone 1-512-471-0476

Main points:

1. Extraordinarily large solution pans were discovered on the Campeche Bank
2. The pans imply a very arid climate in this region during the last glacial period
3. Modern sediment bedforms on the Campeche Bank may be formed by large storms

Published in Continental Shelf Research, v. 117, pp. 57-66, 2016.

Abstract

A high-resolution, near-surface geophysical survey was conducted in 2013 on the Campeche Bank, a carbonate platform offshore of Yucatán, Mexico, to provide a hazard assessment for future scientific drilling into the Chicxulub impact crater. It also provided an opportunity to obtain detailed information on the seafloor morphology and shallow stratigraphy of this understudied region. The seafloor exhibited two morphologies: (1) small-scale (<2 m) bare-rock karstic features, and (2) thin (<1 m) linear sand accumulations overlying the bedrock. Solution pans, circular to oblong depressions featured flat bottoms and steep sides, were the dominant karstic features; they are known to form subaerially by the pooling of rainwater and dissolution of carbonate. Observed pans were 10-50 cm deep and generally 1-8 m wide, but occasionally reach 15 m, significantly larger than any solution pan observed on land (maximum 6 m). These features likely grew over the course of many 10's of thousands of years in an arid environment while subaerially exposed during lowered sea levels. Surface sands are organized into linear bedforms oriented NE-SW, 10's to 100's meters wide, and kilometers long. These features are identified as sand ribbons (longitudinal bedforms), and contained asymmetric secondary transverse bedforms that indicate NE-directed flow. This orientation is incompatible with the prevalent westward current direction; we hypothesize that these features are storm-generated.

Key Words: Carbonate Platform, Solution pans, sand bedforms, Campeche Bank, seafloor, multibeam, CHIRP

1.0 Introduction

Drowned carbonate platforms are found at many of the Earth's continental margins (Schlager, 1981). During sea level low-stands, much of these platforms are subaerially exposed to karstic weathering, subject to the local climatic conditions at those times (Read and Grover, 1977). Subsequent sea level rise will preserved karst features against additional weathering; where the sediment cover is thin, such geomorphology may be exposed at the seafloor and accessible to acoustic surveys (Obrochta et al., 2003). Detailed seafloor mapping over carbonate platforms therefore has the potential to enable investigating ancient karstic morphologies and, by analogy to modern settings, provide an understanding of past climate conditions.

This paper documents such an investigation on the continental shelf of the Yucatán Peninsula, Mexico, also known as the Campeche Bank, a carbonate platform extending into the southern Gulf of Mexico (Figure 1). Aside from the early research by Logan et al. (1969), the Campeche Bank is understudied, particularly in regards to the detailed geomorphology of the vast regions of seafloor between coral reefs. It is unlikely to be featureless. Subaerially exposed by sea level low-stands, the thin sediment veneer to exposed limestone seafloor is apt to exhibit well-preserved karstic landforms (compare, for example, the morphology of the Florida shelf (Obrochta et al., 2003)).

An opportunity to conduct high-resolution mapping of the Campeche Bank seabed was provided in 2013, when the European Consortium for Ocean Research Drilling (ECORD) funded a hazards assessment survey ahead of scientific drilling by the International Ocean Discovery Program (IODP) into the Chicxulub impact crater, roughly half of which extends beneath the offshore Campeche Bank (Gulick et al., 2013). The hazards assessment sought to ascertain the stability of the seafloor and shallow substrate for jack-up drilling operations. It required high-resolution mapping of the seabed morphology and characterization of the shallow sedimentary stratigraphy of the drill sites. This paper is therefore exploratory in nature, an investigation of opportunity in an interesting region that has received little attention in the scientific literature. In particular, the observations provide two avenues of research: fossil karstic geomorphology and modern sedimentary bedforms. Karstic morphology is abundant on the bare-rock exposures at the seafloor, formed in a subaerial environment when the shelf was exposed by lowered sea levels. Such morphology may illuminate surface hydrologic processes and environmental conditions across the peninsula during global glacial conditions. Unconsolidated sediments (carbonate sands) are also distributed throughout the survey area. The bedform morphology of these sediments can provide information on modern hydrodynamic conditions.

1.1 Setting

The Campeche Bank is a broad shelf, covering ~57,000 km^2 and extending ~100-300 km from the shoreline to the shelf break at ~200-300 m water depth with an overall gradient of ~0.0002-0.001 (Logan et al., 1969). Most of the shelf seafloor is composed of indurated, karstic limestone of probable Pleistocene age (Logan et al., 1969). Sedimentary cover from the shoreline to the ~60 m isobath is identified as the Progreso Blanket (Logan et al., 1969), and ranges in thickness from 0 m to around 1 m. With no major drainage systems on the Peninsula, there is very little terrigenous sediment, particularly to the north and east. What deposits do exist in these regions are composed primarily of medium- to fine-grained skeletal carbonate sand, presumably formed by the breakup of skeletal material along the bottom due to wave-current action (Logan et al., 1969). Reef complexes fringe the Campeche bank near the 60 m isobaths (Kornicker and Boyd, 1964; Logan et al., 1969; Blanchon and Perry, 2004), and additional reefs are mapped within the shallower regions of the Progreso Blanket (Zarco-Perelló et al., 2013). Nevertheless, the inner shelf is not a protected, lagoonal setting; rather, it is open to the passage of waves and currents and, like the west Florida shelf, the Campeche Bank is considered to be an "open, deeply submerged inclined shelf", as well as a "high energy" environment (Logan et al., 1969). The Yucatán shelf is typically subjected to westerly currents (Zavala-Hidalgo et al., 2003), and it is frequented by hurricanes and tropical storms (Boose et al., 2003) that can mobilize sand in large quantities.

2.0 Methods

The ECORD survey on the Campeche Bank was conducted through a partnership between the University of Texas Institute for Geophysics (UTIG), the Universidad Nacional Autónoma de México (UNAM), and Seafloor Geotec LLC (SGL). The survey included a broad spectrum of data collection: multibeam bathymetry, side-scan backscatter, CHIRP and boomer acoustic reflection, cone penetrometer, and sediment samples which were analyzed for grain size distribution. It was conducted aboard the UNAM R/V *Justo Sierra* from 16 April to 23 April, 2013, over a study area within the Chicxulub impact crater that encompasses three potential IODP drilling sites. The planned study area covered an area ~10.58 km^2, located ~32 km northwest of Puerto Progreso, Mexico in ~16-18 m water depth (Figure 1). This region is within the sedimentological environment identified as the Progreso Blanket (Logan et al., 1969), and east of the Sissal Reefs mapped by Zarco-Perelló et al. (2013). Survey speeds were typically 4-5 kts for all instrumentation. Primary navigation for the R/V *Justo Sierra* multibeam echosounder was by the Seatex Seapath 200 positioning system. Navigation for all other instrumentation was derived by differential GPS with a base station located in Puerto Progreso.

2.1 Multibeam Echosounder

The R/V *Justo Sierra* is fitted with a hull-mounted Kongsberg EM3002 multibeam echosounder system with data acquisition using the Kongsberg SIS software. The operating frequency of the system is 280-310 kHz. Track density (~70 m) was sufficient to provide >100% coverage in the area of interest. The raw multibeam data were corrected for heave, pitch, roll, and yaw. Sound velocity profile corrections were made based on CTD casts. Tide corrections were performed based on raw data from a year-old tide station installed by UNAM in Puerto Progreso. These data have not yet been calibrated to a specific sealevel datum, which typically takes two years of measurements to calculate (J. Zavala Hidalgo, pers. comm., 2013). Erroneous echosounder pings were manually edited within CARIS software. Navigation data were also edited within CARIS and the multibeam lines were merged and motion data were applied to correct for heave, pitch, roll, and yaw. The final edited data were gridded at 0.00001 by 0.00001 degrees (~1 m) with a vertical resolution of ~10 cm. Topographic profiles were generated for different feature types.

2.2 Side-scan Sonar

The side-scan sonar data were collected using an EdgeTech 2000-DSS dual frequency system, towed simultaneously with multibeam acquisition. Track density (~70 m) and maximum slant range (100 m) were sufficient to provide >200% coverage, allowing for mosaics with uniform look direction. The side-scan sonar system were operated at a frequency of between 385 and 435 kHz, and data were acquired using EdgeTech's Discover software. Calculated layback corrections were input into the topside logging computer and applied to the recorded data. The towfish-generated side-scan data were slant-range corrected to remove the water column along the nadir of the data using CARIS software. These data were then mosaicked using the integrated GPS locations corrected to the towfish position. The mosaicked data were gridded at 0.00001 by 0.00001 degrees (~1 m). Images were made using single-direction illumination at full resolution (0.1 m) to allow for clearer geologic interpretation. However, many important small-scale features that could be observed in the unmosaicked data were irreparably degraded by the stretching and averaging associated with the mosaicking process. We will therefore also present unmosaicked side-scan images data in order to demonstrate these features.

2.3 CHIRP Acoustic Reflection

CHIRP data were collected simultaneously with the side-scan data using the same EdgeTech 2000-DSS instrument. Approximately 435 line kilometers of CHIRP data were acquired. The CHIRP sonar operated at a frequency of 2-15 kHz and acquired using EdgeTech's Discover software. Vertical resolution is ~10 cm. Calculated layback corrections were input into the topside logging computer and applied to the recorded data. A heave filter and fish-depth correction were applied to the data. CHIRP data were interpreted using Landmark Decision Space software. The sole interpretable horizon below the seafloor is the sand/limestone contact.

2.4 Surface-towed boomer

Surface tow boomer (STB) data were collected along ~194 line kilometers. These data have a median frequency of ~400 Hz, and a vertical resolution of ~1 m. Layback was applied during acquisition. STB reflection data are single channel and thus require minimal processing. Data were converted from CODA format to SEGY and then imported into the Paradigm Geophysical

FOCUS seismic processing package. In FOCUS, the amplitudes were laterally balanced but no other filtering or scaling proved necessary. Heave filtering was also applied to improve interpretability of the data. Processed STB data were interpreted using Landmark Decision Space software

2.5 Cone Penetrometer (CPT) and Grab Sampling

The CPT system used is a 2 cm^2 cone penetrometer deployed from a 1300 kg frame. Two attempts were made to collect CPT measurements on seafloor that was interpreted to consist of sand accumulations. However, in each case the CPT head was bent backwards within 10-15 cm of the CPT base, indicating hard bottom at the seafloor or only very minimal sediment cover.

To assess the seafloor sediment in further detail, a series of grab samples using a Smith-McIntyre grab sampler were taken around the IODP scientific drill sites. Carbonate content of sands were tested by submersion in a 10% HCL bath; complete dissolution indicated 100% carbonate content. Grain size analysis was performed by dry sieve for grain size larger than 1 mm, and settling column for grain sizes 1 mm to 64 μm. Visual observations indicated that the samples contain an insignificant (typically <1%) fine (< 63 micron) fraction, and so were not analyzed.

3.0 Results

3.1 Side-scan Backscatter and Grain Size Analysis

The side-scan mosaic (Figure 2) reveals the survey area to be dominated by a NE-SW oriented, linear fabric of alternating high and low backscatter zones, over width scales of 10’s to 100’s of meters and length scales greater than the extent of the survey. The full suite of grain size analysis are shown in the supplemental material. Grab samples 1, 5, 6 and 8 were collected in high-backscatter regions (Figures 2, 3). All of these grabs collected very thin (< 2 cm deep) amounts of sample, indicating an inability of the grab to significantly penetrate the seabed. Grab 8 in particular collected no sediments, returning only living flora and fauna: coral, sea urchin, worms, at least two species of green flora, and a scallop.

Grabs 1, 5 and 6 also returned live flora and fauna along with sparse sediments. These samples included coarse material consisting of whole and broken shells and coral fragments. The high-backscatter regions are therefore interpreted to be fully exposed hardgrounds, or areas of minimal sediment cover, assumed to be carbonate platform rock given the location on the Campeche Bank and documented geology of the Yucatán shelf (Logan et al., 1969; Ahr, 1973).

Grabs 2, 3, 4, 7, 9 and 10 were collected in low-backscatter regions (Figures 2, 3). All these grabs returned, to >4 cm depth, well-sorted fine carbonate sand, with occasional small whole shells, and large foraminifera. The low-backscatter regions are therefore interpreted to be sand accumulations overlying the hardgrounds.

Enlarged, higher-resolution images from the side-scan mosaic (Figure 4) reveal additional details, including variations in backscatter intensity within the sand accumulations, a scarp, and higher-backscatter returns from the base of a channel (these will be further detailed in presentation of bathymetry results in the following section). However, even at the highest-possible resolution (0.1 m), the smallest features observable on the seafloor are poorly imaged. In particular, the high-backscatter, hardground regions of the survey are extensively pitted by shallow, flat-bottomed, circular to oblong depressions that are best observed on unmosaicked, raw data images (Figure 5) rather than the mosaic. Acoustic shadows cast on the nadir-side of the depressions (Figure 5a) indicate that they are steep-walled, possibly vertical. The depressions are typically ~1-8 m width (Figure 5a), but individual depressions can reach 10-15 m wide (Figure 5b), and aggregates (merging of multiple depressions; Figure 5a) can reach sizes of up to 50 m (Figure 5c). The floors of the depression generally exhibit higher backscatter returns than outside the depression (Figure 5), and in some cases exhibit ripples (Figure 5c), providing evidence of coarse-grained unconsolidated sediments, possibly gravel. Where depressions are proximal to sands, we occasionally observe low backscatter returns within the depressions, evidence of partial filling by the fine sands (Figure 5b).

The morphology of the hardground depressions is closely matched to "solution pans" (Ford and Williams, 2007), a karren type of karstification that forms subaerially on bare rock by rainwater-induced dissolution of carbonate. An excellent example of a subaerial solution pan is shown in Figure 6 (Hassiba et al., 2012), observed on limestone outcrops in the Qatar desert. This pan measures ~3 m across and ~20-30 cm deep, with vertical walls, bearing a strong resemblance in size and shape to the smaller depressions imaged acoustically in Figure 5. Solutions pans obtain their distinctive shape by preferentially growing outward, rather than downward, owing to sediment accumulation within the depression (e.g., Figure 6), which inhibits dissolution on the floor while concentrating it on the edges (Cucchi, 2009).

Solution pans are frequently referred to in the literature as "kamenitzas" (e.g., Di Stefano and Mindszenty, 2000; Cucchi, 2009; Hassiba et al., 2012), and less often by numerous other terms largely dependent on where they were observed (see Cucchi, 2009). An early study of solution pans in Texas (Udden, 1925) referred to them as "tinajitas", a local Spanish term for these features that translates to "small water containers." Although this term may be appropriate given the location in Mexican waters, we opt to use "solution pan" as a more generically descriptive term. Solution pans observed on land are, however, considerably smaller than the largest examples observed in this study, typically ranging from a few centimeters to 1-2 m wide, with a maximum observed size of 6 m (Cucchi, 2009). A particularly large example mapped by Udden (1925) in Texas limestone measured ~5 m long, ~3 m wide and ~60 cm deep.

3.2 Multibeam Bathymetry

The overall bathymetry of the survey area is flat-lying, with short-scale variations ranging from ~16 to ~18 m water depth (Figure 7). The sand bedforms observed in the side-scan sonar backscatter intensity data are also observed in the bathymetry (Figures 7, 8) to be topographic highs up to 1 m relief, with morphology organized at two scales. The overall NE-SW trend (also observed on the side-scan sonar backscatter data; Figure 2) constitutes the larger scale, while at smaller scales we observe an orthogonal sand-wave morphology (~20-100 m wavelengths and relief of ~0.2-0.6 m), which are asymmetric with steeper slopes facing NE (Figure 9a). The larger scale morphology can be classified as longitudinal bedforms (ribbons). Such combined longitudinal/transverse bedform morphology is known to be indicative of strong current velocities (Kenyon, 1970).

Hardground regions between the sand bedforms exhibit morphology abundantly pitted by depressions (Figures 7, 8b), consistent with the observations of numerous pans from the unmosaicked side-scan images (Figure 5). A bathymetric profile sampled within the hardground region (Figure 9b), although not well-enough resolved spatially to delineate the steep-walled, flat-bottom pan morphology of the depressions, can nevertheless be used to quantify the vertical relief of these features. From this profile we observe relief of ~0.1 to 0.5 m, values consistent with, for example, the larger subaerial limestone solution pans documented by Udden (1925) and Hassiba et al. (2012; Figure 6).

The morphology in the NW sector of the survey area (Figures 7, 8a), represents a notable departure from the sand bedforms/hard ground fabric that dominates the rest of the survey area. We observe ~1 m-relief scarps, and sinuous, dendritic channels of up to ~2 m of relief that appear to be paleo-flow features. This sector exhibits the strongest topographic variability, with up to 3 m total relief (Figure 7), and is dominated by high-backscatter reflectivity (Figures 2, 4a) indicative of hard grounds. There are, however, surface sands evident in the backscatter (Figures 2, 4a) which are not clearly evident in the bathymetry, indicating that the sand accumulations in this region are likely very thin.

3.3 CHIRP and Boomer Reflection Data

Examination of reflection profiles revealed that the CHIRP data successfully imaged much of the sand bedforms, with detectable sub-seafloor reflections as shallow as ~0.15 ms (twtt) below the seafloor (~13 cm, assuming 1700 m/s acoustic velocity in sediment) that we interpret as the sand/limestone contact (Figure 10). A maximum bedform thickness of ~1.3 ms (~1 m) was measured. Figure 11 displays the interpreted sand isopach values overlain on the side-scan sonar backscatter map. As expected, there is a very strong correspondence between where the sand reflector was imaged and where the low backscatter regions are. Not every sand bedform could be imaged by the CHIRP data, indicating that many accumulations of sand are below the threshold of ~13 cm in thickness required to be imaged. The thickest sands are in the SW sector of the survey area.

With ~1 m vertical resolution, surface tow boomer reflection data were unable to resolve the sand/limestone contact. We were, however, able to image a subsurface reflector, assumed to be a layer within the limestone, ~1-3 m below the seafloor, and dipping slightly north (Figure 12).

This reflector did not otherwise display significant variability in depth throughout the entire study area. In particular, we find no evidence of any significant disruption of the reflector that could be construed as a large karstic collapse structure, such as a cenote, which are common on the Yucatán Peninsula (Connors et al., 1996).

4.0 Discussion

4.1 Karst Development

By their similarity of morphology, and for lack of any plausible alternative explanation, we interpret the bedrock depressions observed on the seafloor in our study as solution pans. However, the formation of solution pans requires a critical condition: that bedrock be subaerially exposed so that rainwater can pool in depressions and dissolve rock downward and outward (Ford and Williams, 2007; Cucchi, 2009). The bedrock cannot be covered with seawater; Campeche Bank solution pans must have formed when the shelf was exposed by lowered sea level. Regionally-proximal sea level curves indicate that, at ~17 m water depth, the survey area was exposed prior to ~9-9.5 ka (Toscano et al., 2011) or ~10 ka (Simms et al., 2007), while global sea level models suggest an age closer to 8.2 ka (Simms et al., 2007). This time frame corresponds to an abrupt sea level rise associated with release of Lake Agasiz waters into the northern Atlantic (Tornqvist and Hijma, 2012). Global sea level curves (e.g., Waelbroek et al., 2002; Siddall et al., 2007) indicate that subaerial exposure at the survey depths extended at least as far back as oxygen isotope stage (OIS) 5.1, ~80 ka, and more likely as far back as OIS 5.5, ~120 ka.

The solution pans observed in this study are extraordinarily large, with single, unmerged examples often reaching sizes of 8 m in width, and occasionally 10-15 m (Figure 5). In contrast, solution pans observed on land have not been observed to exceed 6 m in width (Cucci, 2009). Even with > 100 kyr in exposure time, it is debatable as to whether this duration represents sufficient time to form such large solution pans, due to the low weathering rates of limestone by rainwater dissolution (typically 100ths to 1000ths of a mm/yr (e.g., Smith et al., 1995)). Information on growth rates for solution pans in particular, however, is extremely limited. Cucchi (2009) reports measurements of 0.02-0.03 mm/yr for the lowering rate of solution pans. However, for such extraordinarily large solution pans, the widening rate will be more important than the lowering rate as the base of pan becomes inured to lowering by the detritus that collects within. Rose and Vincent (1986) estimated that a 10 cm deep and 20 cm wide solution pan would require 3260 years to form, which would suggest a widening rate of ~0.06 mm/yr.

Even if we assume a more generous rate of 0.1 mm/yr for outward growth of the Campeche Bank solution pans, an 8 m-wide pan would require 80 kyr years to form, and a 15 m-wide pan would require 150 kyr. It is possible that the larger solution pans could have their origins prior to the OIS 5E highstand ~120 ka. Alternatively, we might postulate, although without any evidence to support it, that solution pans may continue their growth in a marine setting, perhaps by mechanical or biological weathering. In particular, the coarse-grained sediments that evidently reside within the pans could become agitated during storm events, thereby abrading and enlarging the perimeter of the pans.

Solution pan development also requires that bedrock not be covered by soil and vegetation. For such large pans, this implies that the Campeche Bank did not experience significant soil development over a span of 10's of thousands of years while sea level was lowered. Soil development on carbonate substrate is strongly dependent on climate (Isphording, 1978; Bautista et al., 2011). On the Yucatán Peninsula today, strong variations in average rainfall correlate to variations in soil thickness (Isphording, 1978; Bautista et al., 2011). In particular, the northwest coastal plain, directly inshore of the survey area, experiences the driest conditions on the Peninsula (60-100 cm annually), has the thinnest soils (< 50 cm), and bedrock is exposed over 40-60% of the area (Isphording, 1978). Despite the bedrock exposure, solution pans have not, to our knowledge, been reported on land in this region, suggesting that even this amount of soil is sufficient to accumulate in any depression and prevent solution pan evolution. We therefore hypothesize that lowstand climate on the Yucatán Peninsula was more arid than it is today. Possible support for this hypothesis is found in a paleoclimatology study of lacustrine sediments in Lake Quexil, Guatemala (Leyden et al., 1994). Leyden et al. (1994) report that extremely arid conditions existed at that location throughout the last glaciation.

The NW sector of the survey area exhibits a more complex morphology than the alternating ribbon/bare rock morphology elsewhere, including scarps (up to ~1 m relief), deeper pitting (up to ~1 m relief), and sinuous, dendritic channeling (up to ~2 m relief). These observations indicate that a diverse karstic morphology is present on the Campeche Bank, with the weathering effects of both flowing and standing water present. Flowing water could indicate that a period wetter climate also existed sometime during the ~100 ky of subaerial exposure since OIS 5E. Alternatively, it is possible that channel-cutting weathering/erosion of bedrock by surface flow occurred during arid conditions. Examples of such morphology are numerous; they can be driven either by steady spring-fed flows or punctuated floods (e.g., Laity, 2008). A better understanding of this channel system would require a more extensive surface mapping effort to determine form, extent and origin.

4.2 Sand Bedforms

Linear sand bedforms oriented NE-SW, 10's to 100's of meters wide, and <1 m thick, are observed throughout the study area (Figure 2). Within the larger sand bedforms, we observe asymmetric secondary bedforms (~20-100 m wavelengths and relief of ~0.2-0.6 m) with steeper sides facing to the NE (Figure 9b). The bedforms bear a strong morphological similarity to "type C sand ribbons," in size, shape and sand thickness, as described by Kenyon (1970) in a study of bedforms in the North Sea. Sand ribbons are longitudinal bedforms indicative of relatively strong current velocities (Stow et al., 2009). The secondary bedforms indicate that the flow that formed the ribbons was directed to the NE.

Ambient flow directions on the Campeche Bank are westerly at all times of the year (Zavala-Hidalgo et al. 2003), inconsistent with the indicated NE flow direction. We hypothesize that the bedforms are formed during strong flow events, and that ambient current conditions are insufficiently vigorous to remobilize the sand. Some support for this hypothesis is provided by boundary-layer flow measurements on the Campeche Bank by Sternberg (1976). At three locations at 35-46 m water depth on the northern and eastern sides of the Bank, he measured ambient current speeds of 5-18.5 cm/sec at 1 m above the seafloor. Such current speeds are well below the threshold required to transport fine sand (~60-80 cm/sec; Miller et al., 1977). The numerous tropical cyclones that have historically impacted the Campeche Bank (Boose et al., 2003) provide an obvious candidate for such events. For example, a linear string of transverse bedforms, similar to our observations, was documented by Kennedy et al. (2008) to have formed in response to Hurricane Dennis offshore of Panama City, Florida. Tropical storm Dolly (http://www.nhc.noaa.gov/data/tcr/AL042008_Dolly.pdf) is a recent candidate for impacting the survey area. Dolly's track crossed the northern coast of the Yucatán Peninsula in 2008 on a

WNW track; the storm eventually strengthening to a hurricane over the Gulf of Mexico before making landfall again at Brownsville, Texas. As Dolly exited the Campeche Bank region, the survey area would have been in the SE quadrant of the storm, with wind-driven currents from the counterclockwise-rotating cyclone directed to NE. Hurricane Gilbert (Brown et al., 2014), which followed a similar path in 1988, is also a possible candidate.

5.0 Conclusions

The Campeche Bank, on the northern edge of the Yucatán Peninsula, Mexico, is a vast and largely unexplored terrain. It is not, however, featureless. Having been exposed continuously for many tens of thousands of years since the last sea level high-stand, the carbonate platform has experienced substantial karstic weathering that was preserved after inundation by rising sea level, and kept exposed at the seafloor by non-depositional conditions. Solution pans in particular are observed nearly everywhere in our survey area not covered by sand. Most individual solutions pans observed in our study area are 1-8 m in width, but a few are as large as 15 m in width and, where multiple pans have merged together, the aggregated depressions can reach 50 m in width. The great size of these solutions pans implies that the Campeche Bank was subaerially exposed with soil free conditions for a very long time. The larger solution pans are likely to have been in development for many 10’s of thousands of years, and possibly well over 100 kyr. The lack of soil development over such a long time frame suggests very arid paleoclimatological conditions on the Yucatán Peninsula during glacial periods.

Additional bedrock morphology observed in our study area includes flow channels up to 2 m deep, and scarps up to 1 m tall. These features suggest a rich diversity of karstic landforms on the Campeche Bank that will require additional survey work to explore and investigate origins and timing.

A thin (< 1 m) cover of fine carbonate sands is also observed in the survey area. These sands are organized into highly linear bedforms oriented NE-SW, 10's to 100's of meters wide, and kilometers long (the length scale exceeds the survey extent), with exposed bedrock between the sand bedforms. Within the larger bedforms we observe secondary bedforms with a scalloped plan view and asymmetric cross section, with steeper slopes facing the NE. This morphology is indicative of sand ribbons formed under a NE-directed flow regime. In contrast, the ambient, year-round current direction in the vicinity of the survey region is westward; we suggest instead that the sand ribbons formed during a cyclonic storm.

Acknowledgements

Data acquisition was funded by the European Consortium for Ocean Research Drilling. We thank the captain, Leobardos Rios, and crew of the R/V *Justo Sierra* for their hard work and dedication to the success of the survey. This is UTIG contribution number XXXX. The UNAM project number is IG-101112. The data from the Chicxulub Hazard Site Survey is open, but restricted. To access the data, users should apply to the ECORD Science Operator (eso@bgs.ac.uk), stating the purpose for which the data will be used. Users of the data are obliged to acknowledge ECORD in any publications or outputs.

References

Ahr, W. M, 1973. The carbonate ramp: An alternative to the shelf model. Gulf Coast Assn. Geol. Soc. Trans. 23, 221-225.

Bautista, F., Palacio-Aponte, G., Quintana, P., Zinck, J.A., 2011. Spatial distribution and development of soils in tropical karst areas from the Peninsula of Yucatan, Mexico. Geomorph. 135, 308-321.

Blanchon, P., Perry, C.T., 2004. Taphanomic differencitaion of Acropora palmate facies in cores from Campeche Bank reefs, Gulf of México. Sedimentology 51, 53-76.

Boose, E.R., Foster, D.R., Barker Plotkin, A., Hall, B., 2003. Geographical and historical variation in hurricanes across the Yucatán Peninsula. In: Gomez-Pompa, A., Allen, M.F., Fedick, S.L., Jimenez-Osornio, J.J. (Eds.), The Lowland Maya: Three Millennia at the Human–Wildland Interface. Haworth Press, Binghamton, NY, pp. 495–516.

Brown, A.L., Reinhardt, E.G., Van Hengstum P.J., Pilarczyk, J.E., 2014. A coastal Yucatan sinkhole records intense hurricane events. J. Coast. Res. 30, 418-428.

Connors, M., Hildebrad, A.R., Pilkington, M., Ortiz-Aleman, C., Chavez, R.E., Urrutia-Fucugauchi, J., Graniel-Castro, E., Camara-Zi, A., Vasquez, J., Halpenny, J.G., 1996. Yucatán karst features and the size of Chicxulub crater. Geophys. J. Int. 127, F11-F14.

Cucchi, F., 2009. Kamenitzas. In: Gines, A., Knez, M., Slabe, T., Dreybrodt, W. (Eds.), Karst Rock Features - Karren Sculpturing. ZRC Publishing, Ljubljana, pp. 139-150.

Di Stefano, P., Mindszenty, A., 2000. Fe-Mn-encrusted “kamenitza” and associated features in the Jurassice of Monte Kumeta (Sicily): subaerial and/or submarine dissolution? Sed. Geol. 132, 37-68.

Ford, D., Williams, P., 2007. Karst Hydrogeology and Geomorphology. Wiley, Hoboken.

Gulick, S.P.S., Christeson, G.L., Barton, P.J., Grieve, R.A.F., Morgan, J.V., Urrutia-Fucugauchi, J., 2013. Geophysical characterization of the Chicxulub impact crater. Rev. Geophys. 51, 31-52.

Hassiba, R., Cieslinski, G.B., Chance, B., Al-Naimi, F.A., Pilant, M., M.W. Rowe, 2012. Determining the age of Qatari Jabal Jassasiyah petroglyphs. QScience Connect 4, doi: 10.5339/connect.2012.4.

Isphording, W.C., 1978. Mineralogical and physical properties of Gulf coast limestone soils. Trans. Gulf Coast Assoc. Geol. Soc. 28, 201-214.

Kennedy, A.B., Slatton, K.C., Hsu, T.-J., Starek, M.J., Kampa, K., 2008. Ephemeral sand waves in the hurricane surf zone. Mar. Geol. 250, 276-280.

Kenyon, N. H., 1970. Sand ribbons of European tidal seas. Mar. Geol. 9, 25-39.

Kornicker, L.S., Boyd, D.W., 1964. Shallow-water geology and environments of Alacran Reef Complex, Campeche Bank, Mexico. Bull. Am. Ass. Petr. Geol. 46, 640-673.

Laity, J., 2008. Desert and Desert Environments. Wiley-Blackwell, Hoboken.

Leyden, B.W., Brenner, M., Hodell, D.A., Curtis, J.H., 1994. Orbital and internal forcing of climate on the Yucatan Peninsula for the past ca. 36 ka. Paleogeogr. Paleoclim. Paleoecol. 109, 193-210.

Logan, B.W., Harding, J.L., Ahr, W.M., Williams, J.D., Snead, R.G., 1969. Carbonate sediments and reefs, Yucatán Shelf, Mexico. Am. Assoc. Pet. Geol., Mem. 11, 1-128.

Miller, M.C., Mcnave, I.N., Komar, P.D., 1977. Threshold of sediment motion under unidirectional currents. Sedimentology 24, 507-527.

Obrachta, S.P., Duncan, D.S., Brooks, G.R., 2003. Hardbottom development and significance to the sediment-starved west-central Florida inner continental shelf. Mar. Geol. 200, 291-306.

Read, J.F., Grover, G.A., 1977. Scalloped and planar erosion surfaces, Middle Ordovician limestones, Virginia: Analogues of Holocene exposed karst or tidal rock platforms. J. Sed. Petr. 47, 956-972.

Rose, L., Vincent, P.J., 1986. The kamenitzas of Gait Barrows National Nature Reserve, north Lancashire, England, in New Directions. In Paterson, K., Sweeting, M.M. (Eds.), Karst. Geobooks, Norwich, pp. 473-496.

Schlager, W., 1981. The paradox of drowned reefs and carbonate platforms. Geol. Soc. Am. Bull. 92, 197-211.

Sidall, M., Chappell, J., Potter, E.-K., 2007. Eustatic sea level during past interglacials. In: Sirocko, F., Claussen, M., Sanchez-Goni, M.F. (Eds.), The Climate of Past Interglacials, Development in Quaternary Sciences Volume 7. Elsevier, Amsterdam, pp. 75-92.

Simms, A.R., Lambert, K., Purcell, A., Anderson, J.B., Rodriguez, A.B., 2007. Sea-level history of the Gulf of Mexico since the Last Glacial Maximum with implications for the melting history of the Laurentide Ice Sheet. Quat. Sci. Rev. 26, 920-940

Smith, D.I., Greenaway, M.A., Moses, C., Spate, A.P., 1995. Limestone weathering in Eastern Australia, Part 1: Erosion rates. Earth Surf. Proc. Landf. 20, 451-463.

Sternberg, R.W., 1976. Measurements of boundary-layer flow and boundary roughness over Campeche Bank, Yucatan. Mar. Geol. 20, M25-M31.

Stowe, D.A.V., Javier Hernandez-Molina, F., Llave, E., Sayo-Gil, M., Diaz del Rio, V., Branson, A., 2009. Bedform-velocity matrix: The estimation of bottom current velocity from bedform observations. Geology 37, 327-330.

Tornqvist, T.E., Hijma, M.P., 2012. Links between early Holocene ice-sheet decay, sea-level rise and abrupt climate change. Nat. Geosci. 5 601-606.

Toscano, M.A., Peltier, W.R., Drummond, R., 2011. ICE-5G and ECE-6G modesl of postglacial sea-level history applied to the Holocene coral reef record of northeastern St. Croix, U.S.V.I: investigating the influence of rotational feedback on GIA processes at tropical latitudes. Quat. Sci. Rev. 30, 3032-3042.

Udden, J.A., 1925. Etched potholes. Univ. Tex. Bull. 2509, 5-9.

Waelbroek, C., Labeyrie, L., Michel, E., Duplessy, J.C., Mcmanus, J.F., Lambeck, K., Balbon, E., Labracherie, M., 2002. Sea-level and deep water temperature changes derived from benthic foraminifera isotopic records. Quat. Sci. Rev. 21, 295-305.

Zarco-Perelló, S., Mascaró, M., Garza-Pérez, R., Simoes, N., 2013. Topography and coral community of the Sisal Reefs, Campeche Bank, Yucatán, México. Hidrobiológica 23, 28-41.

Zavala-Hidalgo, J., Morey, S.L., O'Brien, J.J., 2003. Seasonal circulation on the western shelf of the Gulf of Mexico using a high-resolution numerical model. J. Geophys. Res. 108, doi:10.1029/2003JC001879.

Figure Captions

Figure 1. Location of survey area, overlain on regional bathymetry (derived from ETOPO5 (http://www.ngdc.noaa.gov/mgg/global/etopo5.html). Depth contours are in meters. The dock at Puerto Progreso, Mexico, is indicated by heavy line in the lower right of the image; it is ~20 nm from the survey box. Inset shows location of map on the northwest coast of the Yucatán Peninsula, in the Gulf of Mexico.

Figure 2. Side-scan sonar backscatter map generated from east-looking illumination direction only, gridded at 0.00001 by 0.00001 degrees (approximately 1 m). Lighter shades indicate higher backscatter intensities. Grab sample locations G1-G10 are identified, as well as locations for Figures 4, 5 and 10. A notable offset in the middle of the survey area corresponds to the boundary between northward (right) and southward (left) run lines, and thus likely indicates a small error in the estimated layback value.

Figure 3. Grain size histograms estimated for the selected grab sample sediments, one from a low-backscatter region (Grab 3) and the other from a high-backscatter region (Grab 5). Locations shown on Figure 2.

Figure 4. Full-resolution (0.1 m grid spacing) side-scan sonar mosaic images of selected regions, showing strong contrast regions of low backscatter intensities, which are found to be sand accumulations, and areas of higher backscatter intensity, which indicate regions of exposed rock. Also identified are a scarp and a channel (a) that are observed in the bathymetry (see also Figure 8a). Location shown on Figure 2.

Figure 5. Selected raw side-scan images, displaying pitted morphology otherwise poorly imaged after the mosaicking process. The scale bar is accurate for the horizontal (cross-swath) direction. The along-track direction is originally specified in time. However, by comparison with the mosaic (Figure 2), we have rescaled the image so that the vertical spatial scale is approximately that of the horizontal scale. (a) Shallow, flat-bottomed, semicircular depressions. A linear sand bedform is observed at the bottom of the image. (b) Some of the largest single depressions, up to 15 m wide. At least two depressions have been partially filled by mobilized sediments highlighted by lower backscatter intensities. (c) Merged depressions. Ripples are also observed in the depression bottoms, indicating the presence of loose, coarse sediment rather than exposed rock. Locations shown in Figure 2.

Figure 6. Photograph of a solution pan within limestone outcrop of the Qatar desert (Hassiba et al., 2012). Based on the people for scale, we estimate the feature is ~3 m wide and 20-30 cm deep, with vertical sides. The size and shape are similar to many of the depressions imaged in Figure 5.

Figure 7. Color-contoured multibeam bathymetry, artificially illuminated from the north, gridded at 0.00001 by 0.00001 degrees (~1 m). Locations for Figures 8, 9 and 12 are indicated.

Figure 8. Detailed multibeam bathymetry examples of selected regions. Conspicuous features identified include (a) a number of scarps and a channel that are also observed in the side-scan

mosaic (compare Figure 4a), and (b) longitudinal sediment bedforms and pitted morphology (compare Figure 4b). Locations shown on Figure 7.

Figure 9. Topographic profiles through (a) sand bedforms and (b) pitted morphology. The sand bedform profile (a) exhibits ~20-50 cm-tall, asymmetric bedforms, with steeper sides to the NE. Relief of the depressions ranges from ~10-50 cm. Locations shown in Figure 7.

Figure 10. Uninterpreted (top) and interpreted (bottom) CHIRP profile through a sand bedform. The base of the sand bedform is observed as a reflection ~0.3-0.6 ms (~25-50 cm, assuming 1700 m/s speed of sound in sediment) below the seafloor. Location is shown in Figures 2 and 11.

Figure 11. Sand isopach data overlain on side-scan sonar backscatter data. Location of Figure 10 is indicated.

Figure 12. Examples of heave-compensated surface tow boomer reflection data with penetrations up to a few meters subsurface. The upper unit between the seafloor and first reflector is 1-3 m thick (assuming an acoustic velocity of 2000 m/s speed of sound in bedrock). The ~2 m-deep channel feature located on (b) lacks any underlying deeper root. Locations shown in Figure 2.

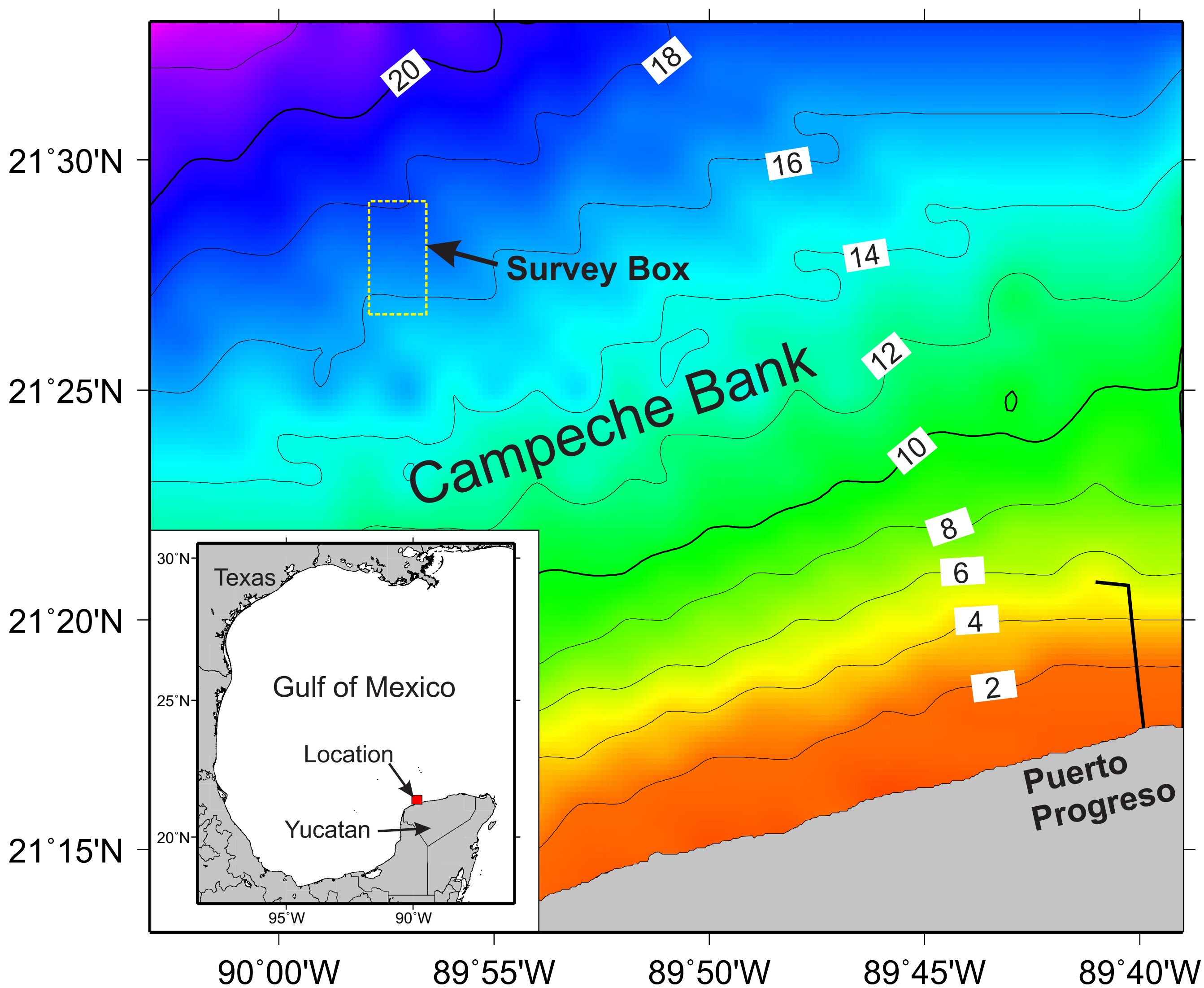

20
18
16
14
12
10
8
6
4
2
Survey Box
Campeche Bank
Puerto Progreso
21˚30'N
21˚25'N
21˚20'N
21˚15'N
90˚00'W
89˚55'W
89˚50'W
89˚45'W
89˚40'W
Texas
Gulf of Mexico
Location
Yucatan
30˚N
25˚N
20˚N
95˚W
90˚W

Figure 1

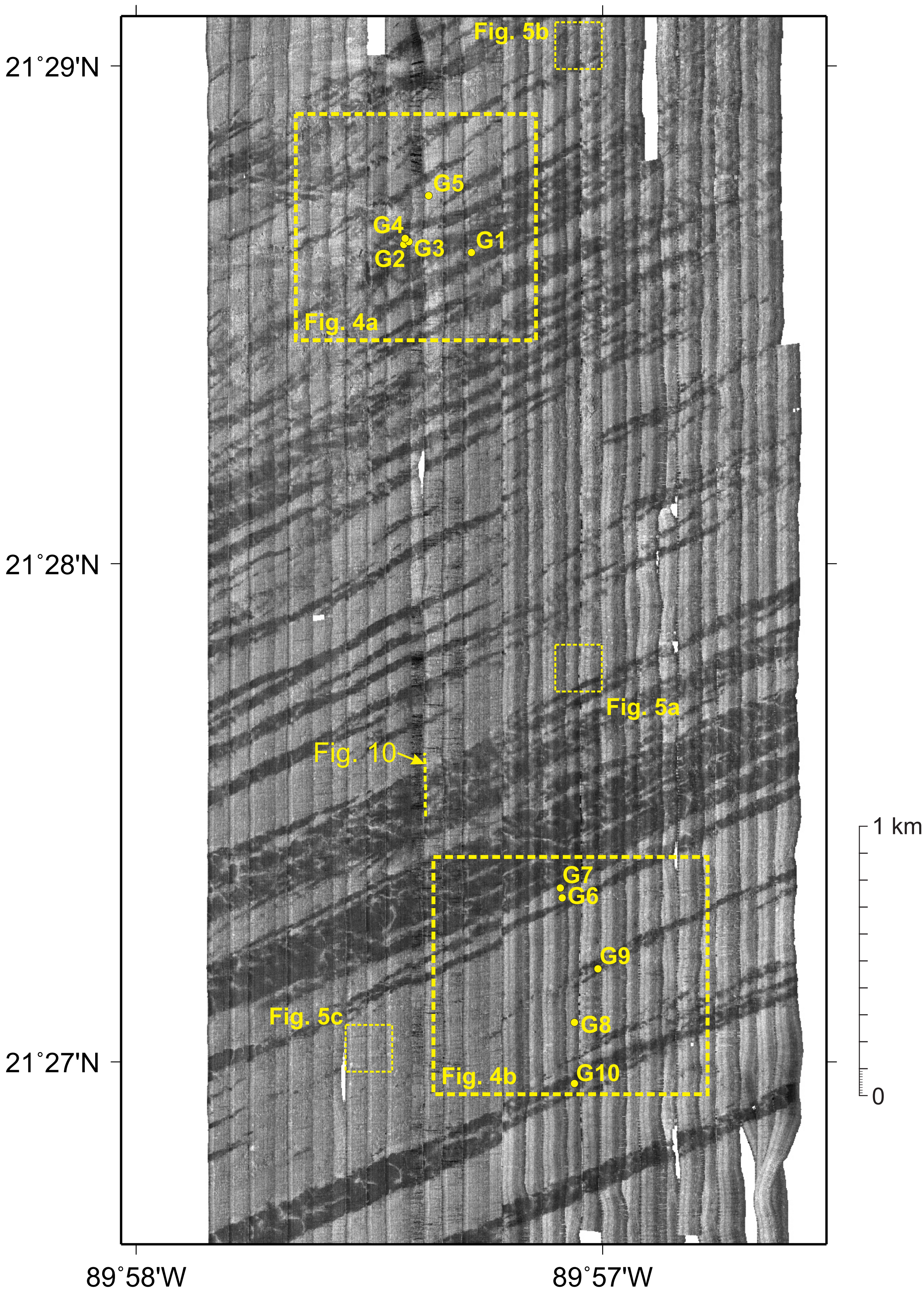

21°29'N
21°28'N
21°27'N
89°58'W
89°57'W
Fig. 5b
Fig. 4a
G5
G4
G3
G2
G1
Fig. 5a
Fig. 10
1 km
0
G7
G6
G9
G8
G10
Fig. 5c
Fig. 4b

Figure 2

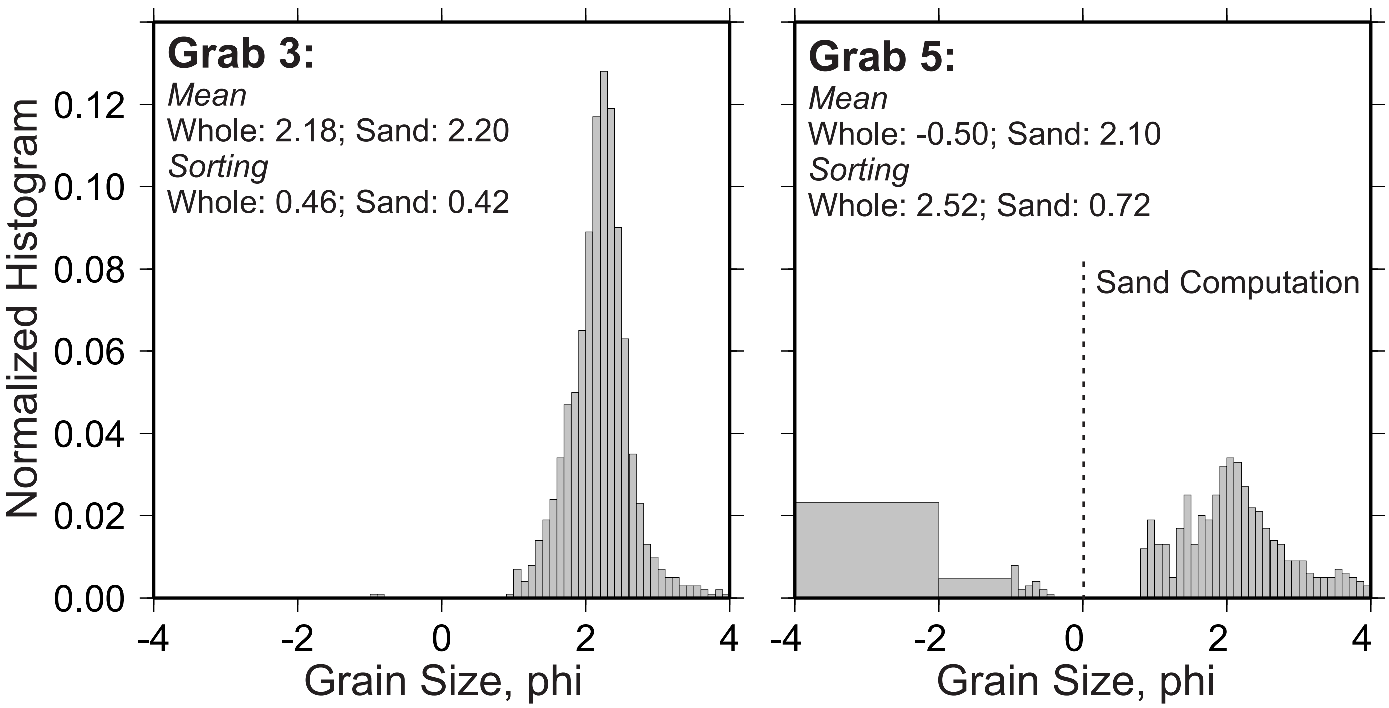
Grab 3:
Mean
Whole: 2.18; Sand: 2.20
Sorting
Whole: 0.46; Sand: 0.42
Grab 5:
Mean
Whole: -0.50; Sand: 2.10
Sorting
Whole: 2.52; Sand: 0.72
Sand Computation
Normalized Histogram
0.12
0.10
0.08
0.06
0.04
0.02
0.00
-4
-2
0
2
4
Grain Size, phi
Grain Size, phi

Figure 3

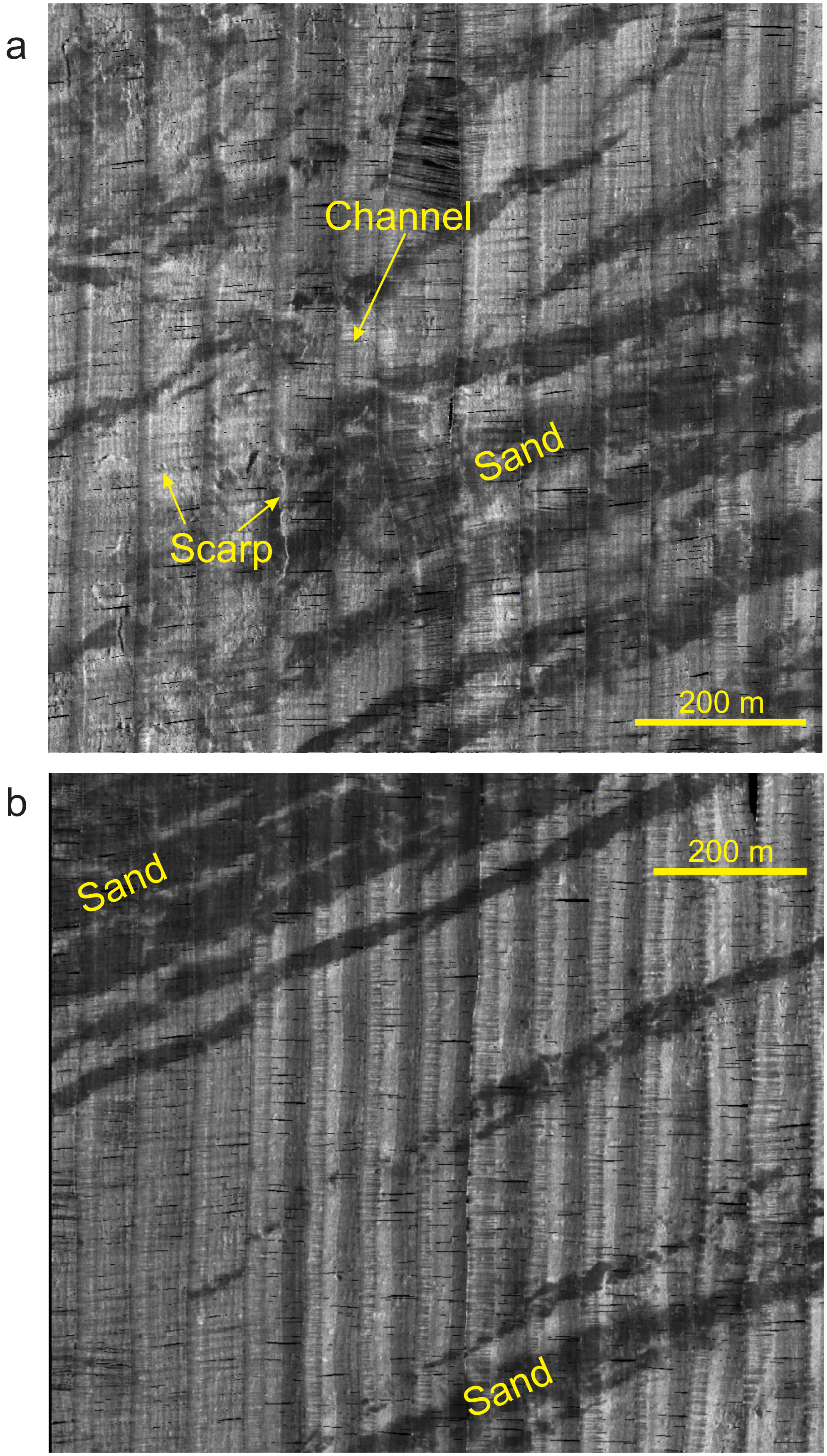

Figure 4

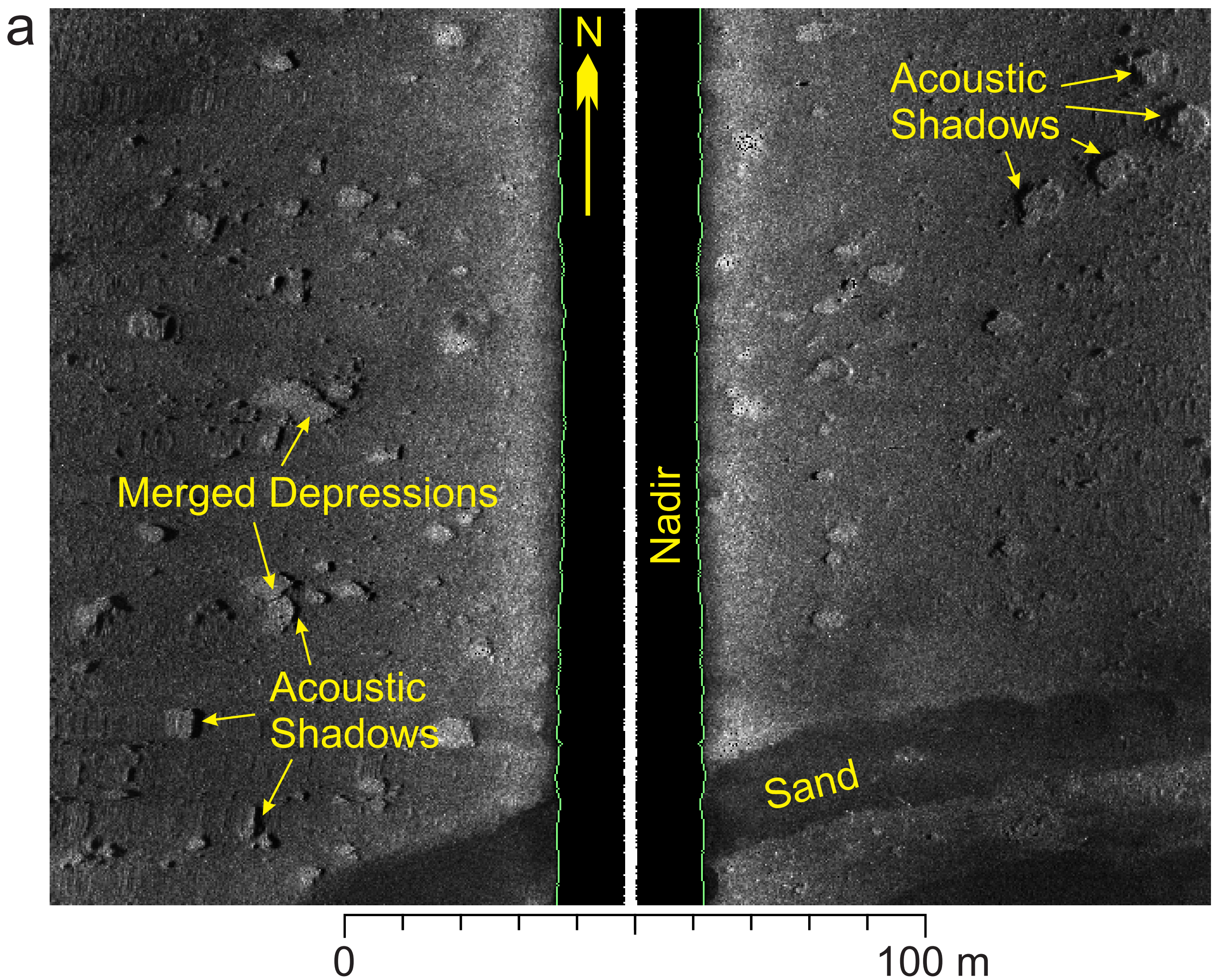
a
N
Acoustic
Shadows
Merged Depressions
Nadir
Acoustic
Shadows
Sand
0
100 m

Figure 5a

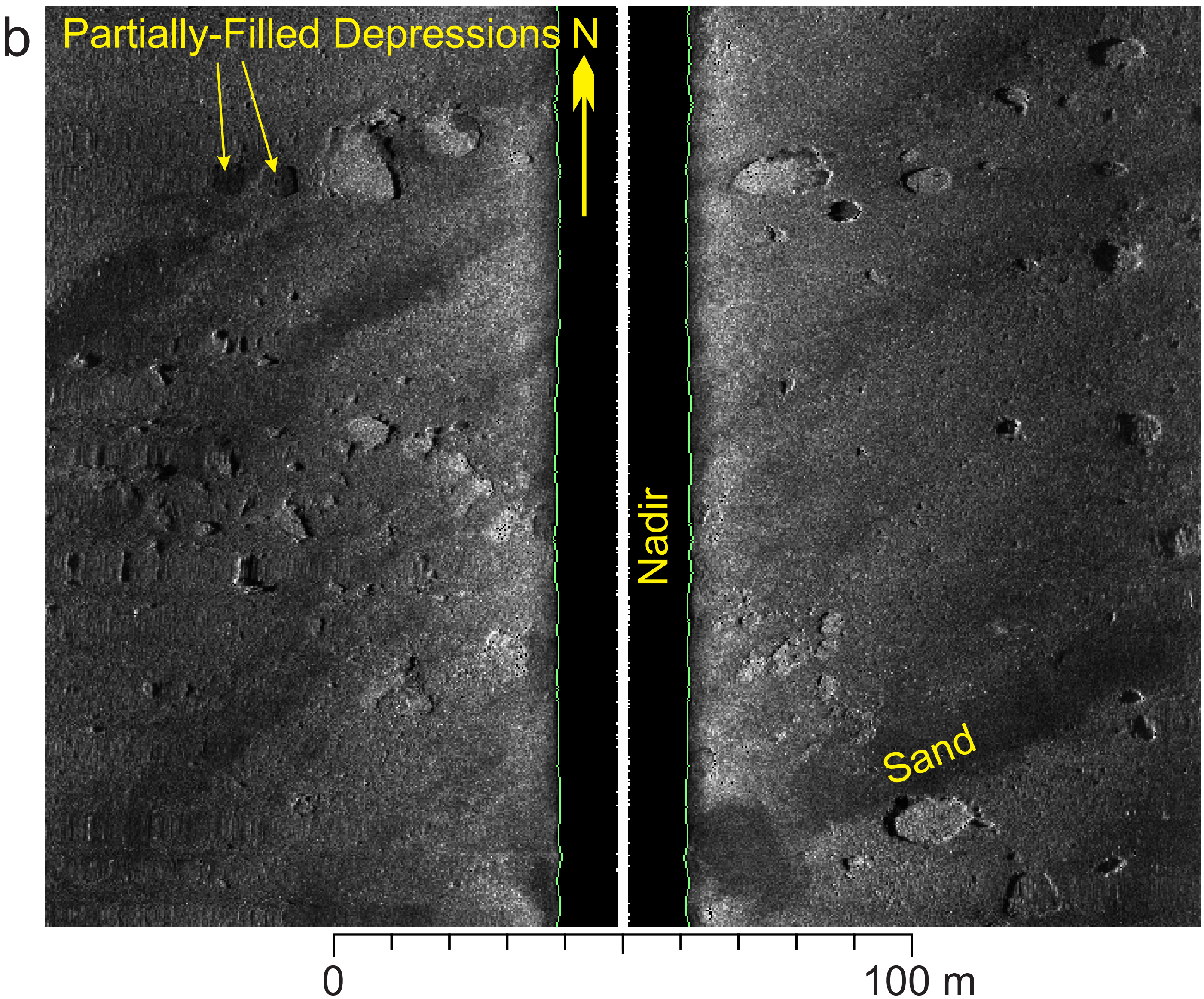

Figure 5b

c

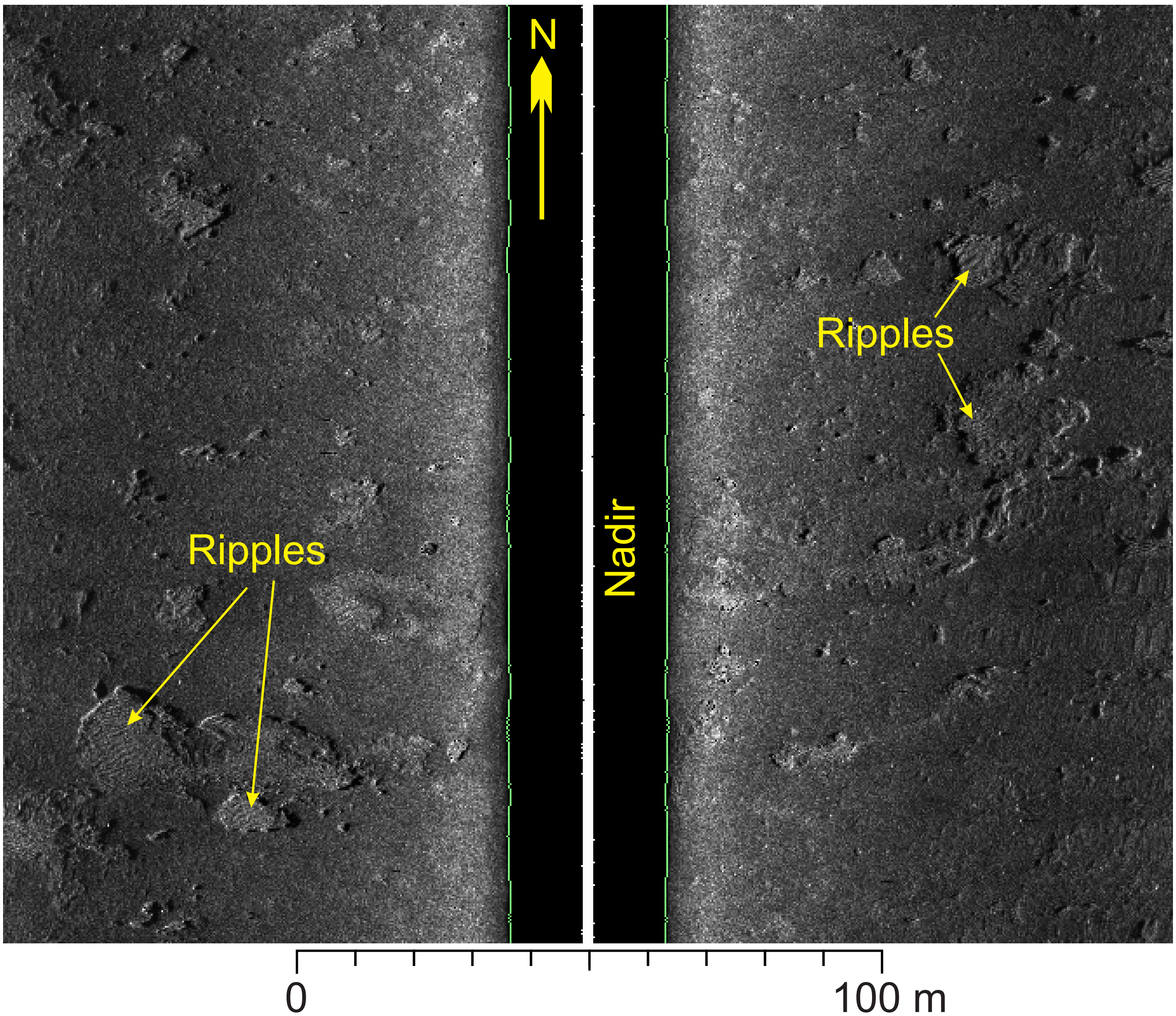

Figure 5c

Figure 6

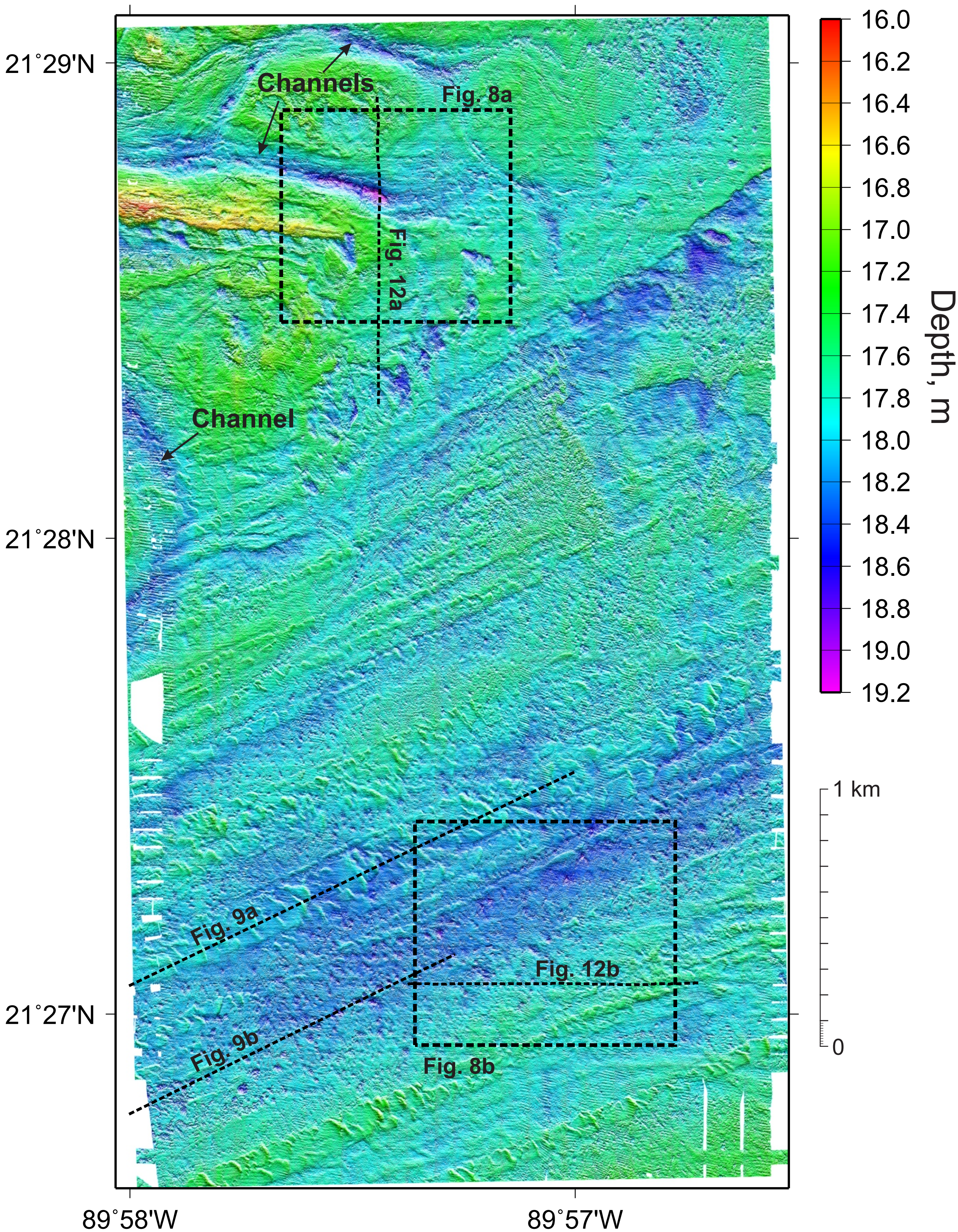
Channels
Fig. 8a
Fig. 12a
Channel
Fig. 9a
Fig. 9b
Fig. 12b
Fig. 8b
21°29'N
21°28'N
21°27'N
89°58'W
89°57'W
16.0
16.2
16.4
16.6
16.8
17.0
17.2
17.4
17.6
17.8
18.0
18.2
18.4
18.6
18.8
19.0
19.2
Depth, m
1 km
0

Figure 7

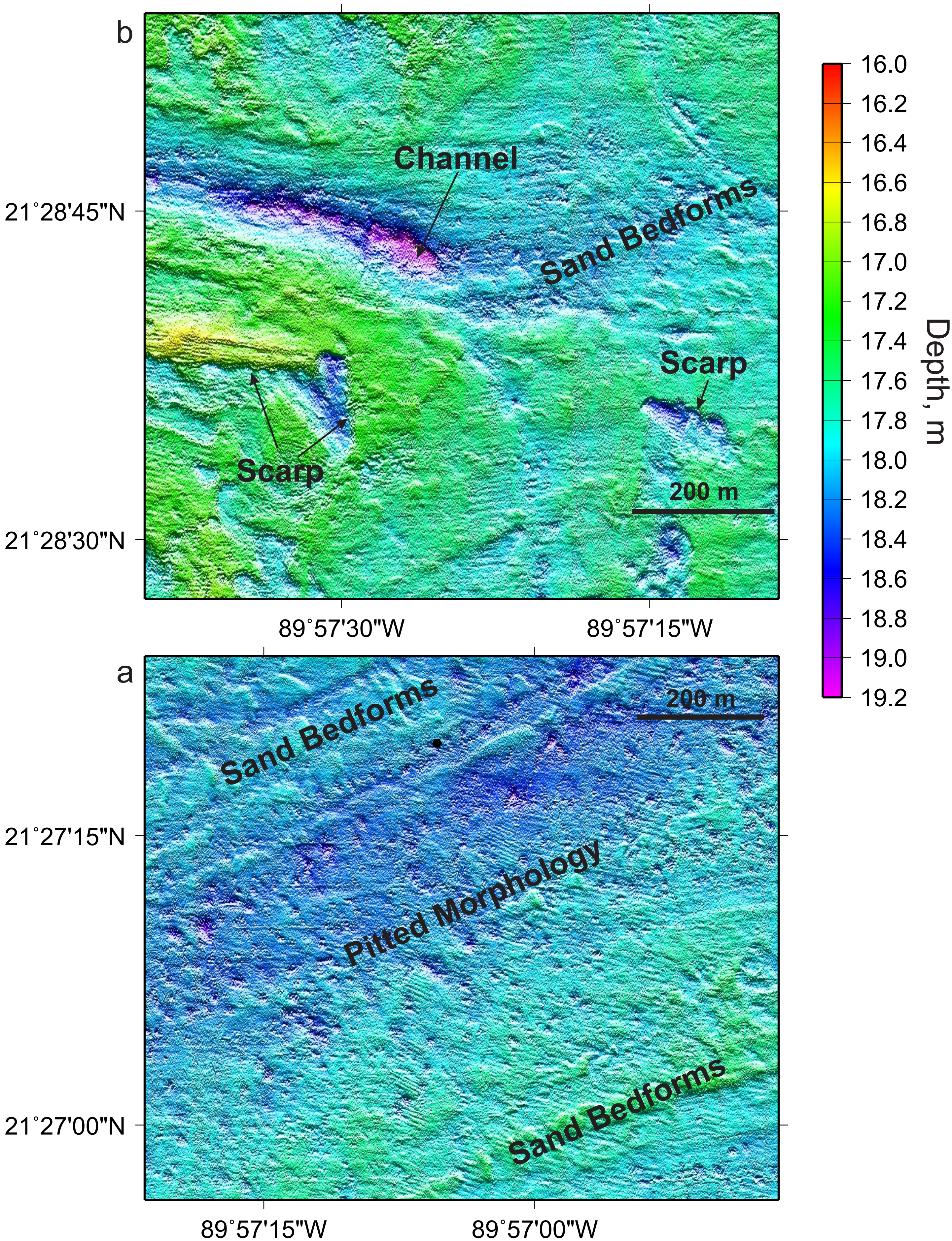

b
Channel
Sand Bedforms
Scarp
Scarp
200 m
21°28'45"N
21°28'30"N
89°57'30"W
89°57'15"W
a
Sand Bedforms
200 m
Pitted Morphology
Sand Bedforms
21°27'15"N
21°27'00"N
89°57'15"W
89°57'00"W
16.0
16.2
16.4
16.6
16.8
17.0
17.2
17.4
17.6
17.8
18.0
18.2
18.4
18.6
18.8
19.0
19.2
Depth, m

Figure 8

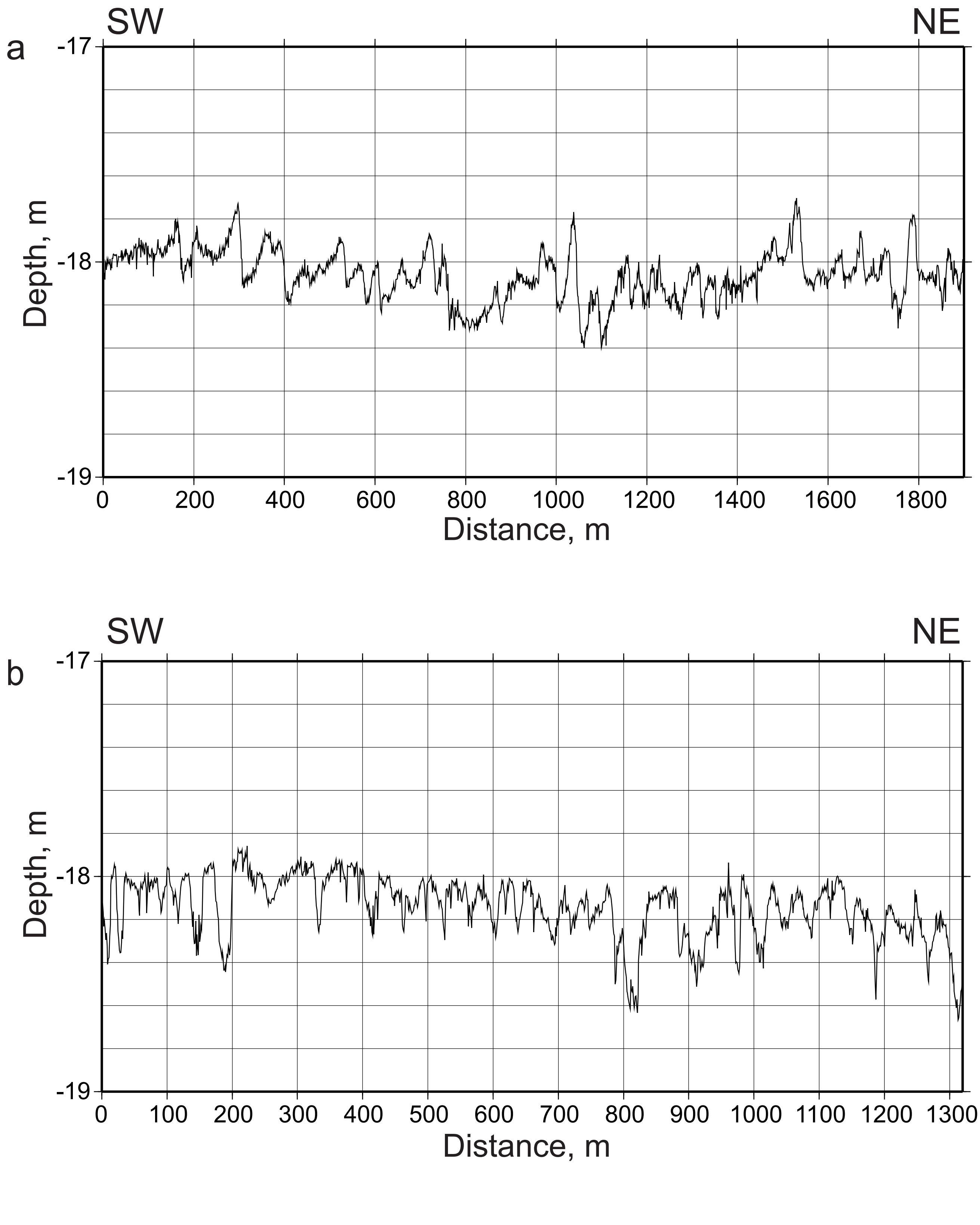
SW
NE
a
-17
-18
-19
Depth, m
0
200
400
600
800
1000
1200
1400
1600
1800
Distance, m
SW
NE
b
-17
-18
-19
Depth, m
0
100
200
300
400
500
600
700
800
900
1000
1100
1200
1300
Distance, m

Figure 9

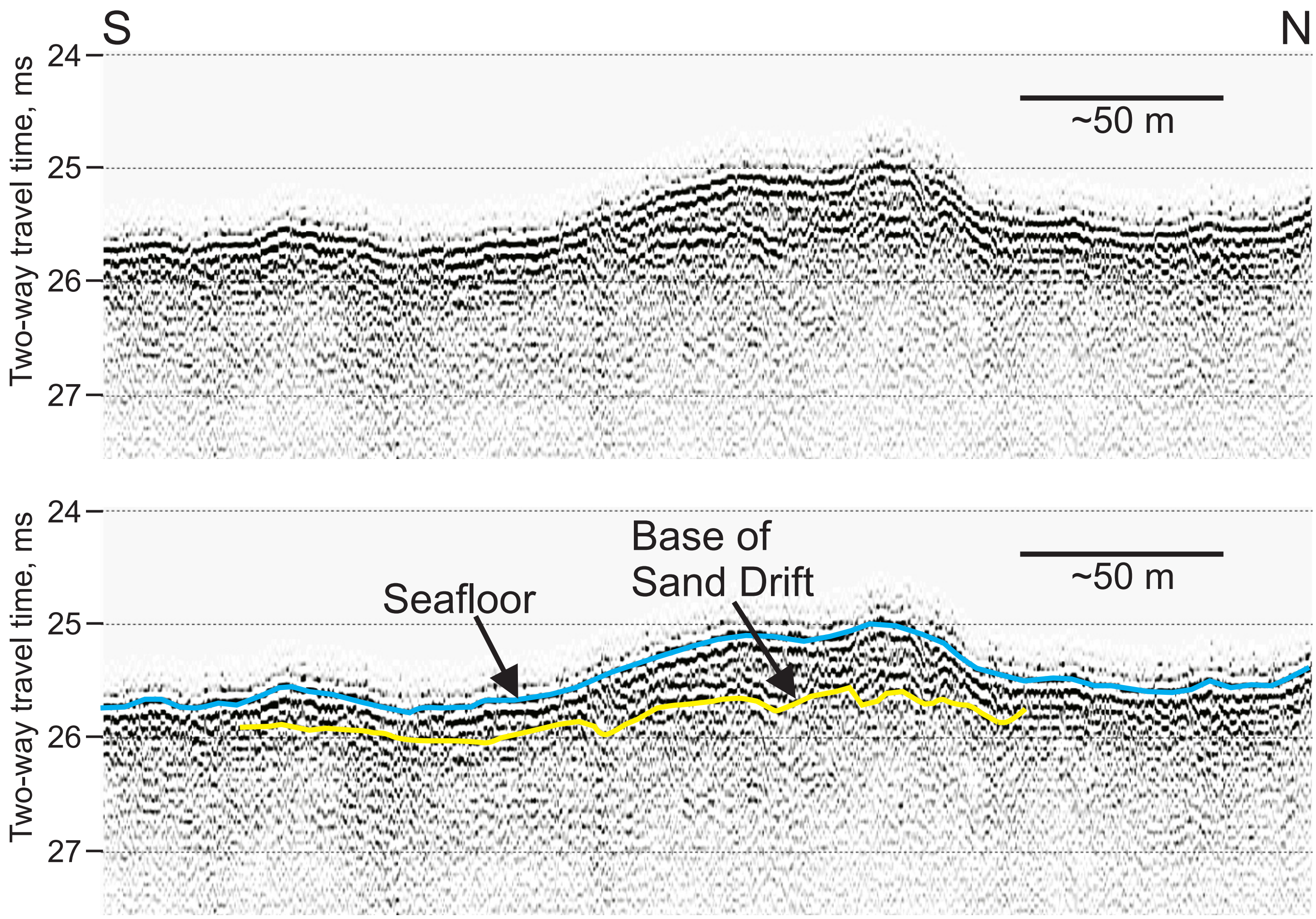
S
N
24
25
26
27
Two-way travel time, ms
~50 m
24
25
26
27
Two-way travel time, ms
~50 m
Seafloor
Base of
Sand Drift

Figure 10

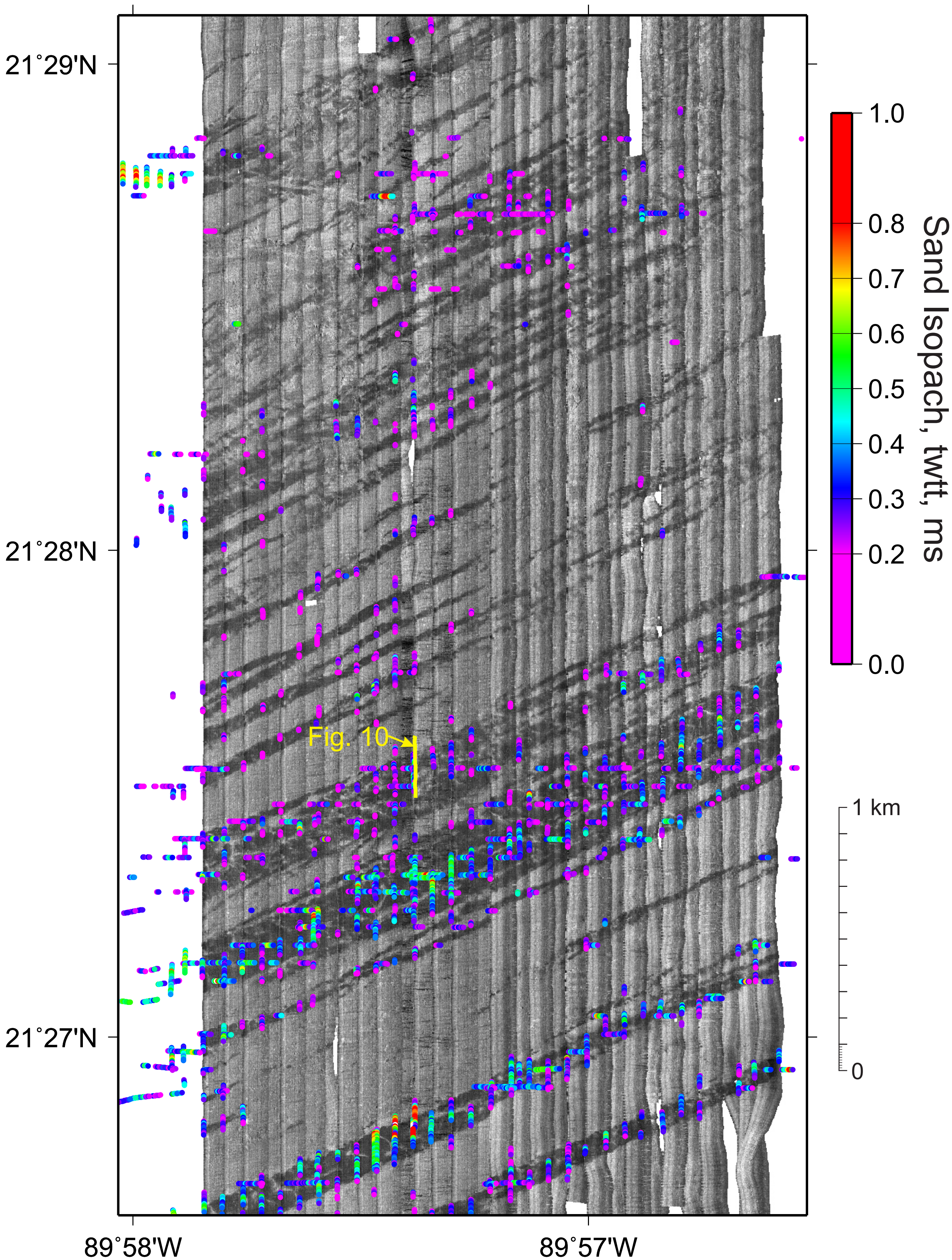

21˚29'N
21˚28'N
21˚27'N
89˚58'W
89˚57'W
Fig. 10
1.0
0.8
0.7
0.6
0.5
0.4
0.3
0.2
0.0
Sand Isopach, twt, ms
1 km
0

Figure 11

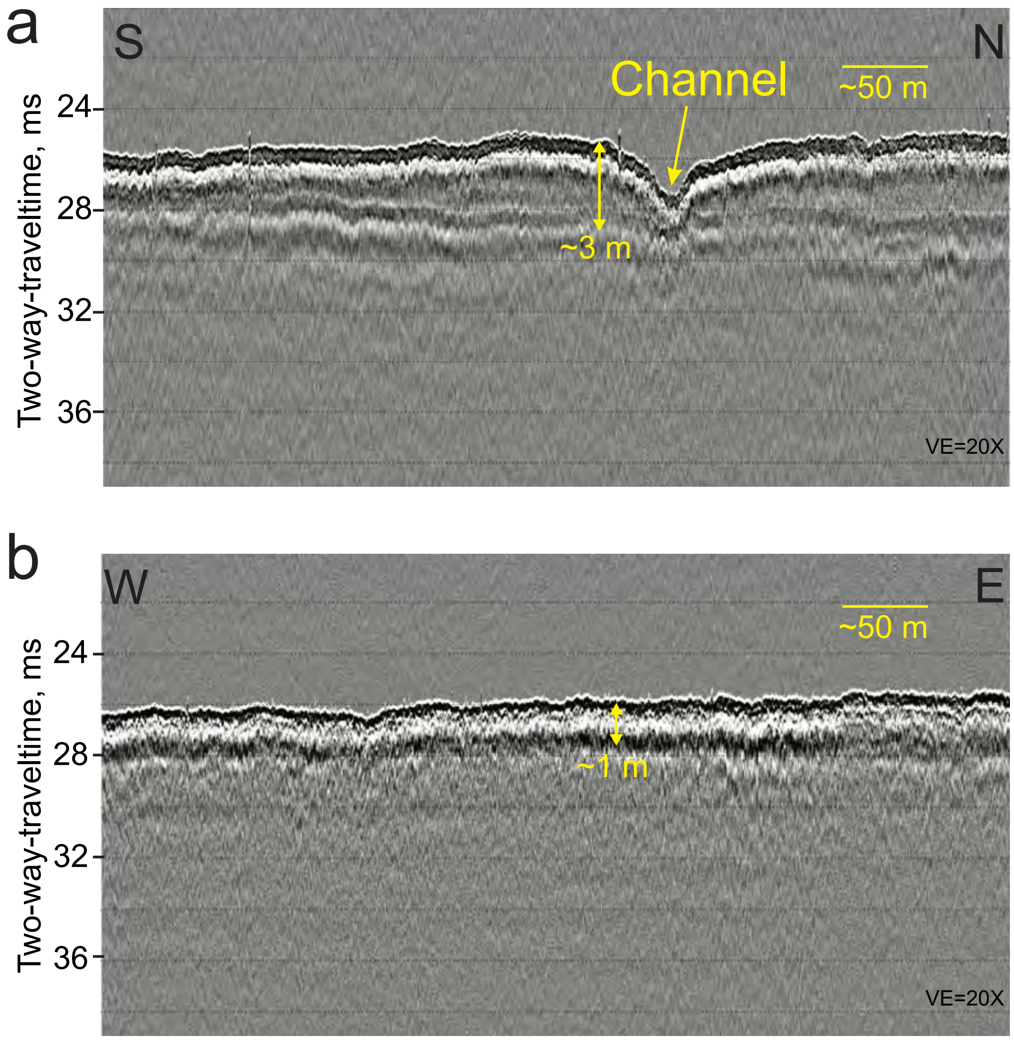
a
S
N
Channel
~50 m
Two-way-traveltime, ms
24
28
32
36
~3 m
VE=20X
b
W
E
~50 m
Two-way-traveltime, ms
24
28
32
36
~1 m
VE=20X

Figure 12